2020 IEEE International Conference on Robotics and Automation (ICRA)
31 May - 31 August, 2020. Paris, France

Versatile Trajectory Optimization Using a LCP Wheel Model for Dynamic Vehicle Maneuvers

Guillaume Bellegarda and Katie Byl

Abstract— **Car models have been extensively studied at varying levels of abstraction, and planning and executing motions under ideal conditions is well researched and understood. For more aggressive maneuvers, for example when drifting or skidding, empirical and/or discontinuous friction models have been used to explain and approximate real world contact behavior. Separately, contact dynamics have been extensively studied by the robotics community, often times formulated as a linear complementarity problem (LCP) for dynamic multi-rigid-body contact problems with Coulomb friction cone approximations. In this work, we explore the validity of using such an anisotropic Coulomb friction cone to model tire dynamics to plan for vehicle motion, and present a versatile trajectory optimization framework using this model that can both avoid and/or exploit wheel skidding, depending on the cost function and planning horizon. Experimental evidence of planning and executing dynamic drift parking is shown on a 1/16 scale model car.**

I. Introduction

Vehicle dynamics have been well studied at varying levels of abstraction. These range from simple models such as kinematic and dynamic bicycle models with few state variables, to a popular high fidelity vehicle dynamics simulator, CarSim, which uses over 250 state variables to estimate full vehicle dynamics. Ideally, the simplest model that still accurately captures the true dynamics is desired for planning and control purposes.

In this work, we specifically consider dynamic vehicle maneuvers involving skidding/drifting. There have been a number of recent works in this area involving both sustained and transient drift. Of note are the different models used as well as the (mostly) decoupling of planning and control with a variety of techniques.

For general vehicle motion planning, Borrelli et al. [1] note that a bicycle model with constant normal tire loads captures most of the relevant nonlinearities associated with lateral stabilization of the vehicle, and present an MPC based approach to active steering, such as used during lane changes, showing results in simulation. Kong et al. [2] studied using kinematic and dynamic vehicle models for autonomous driving with MPC, noting the kinematic model is both computationally less expensive as well as avoids the singularity of popular tire models, and can thus be used at low speeds. A recently proposed vehicle model interpolates between the kinematic and dynamic bicycle models in hand-tuned velocity ranges in an MPC framework to follow a race track for an autonomous car [3].

Kolter et al. [4] remarked that over short periods of time, even complex dynamics such as a car while skidding are often remarkably deterministic. With this intuition they developed a mixed open-loop and closed-loop control framework using a probabilistic method called multi-model LQR, which they applied on a real vehicle for a sliding parking maneuver. The vehicle model for normal driving was learned from experimental data from real driving, and the system was provided with a demonstration of the desired maneuver.

Other works adopting mixed open-loop closed-loop control include [5], [6]. These works study drift parking and cornering, and use a rule-based algorithm to plan a reference trajectory. In [7] the authors divide the cornering problem into free, transit, and drifting regions; where path planning is done by an RRT and rule-based method, with a PI controller for the transit segment. A mixed open-loop closed-loop controller is used to track the trajectory, and the authors validate their methods in CarSim and/or on the BARC car model.

Other works incorporating sampling-based methods for planning include [8], [9]. In [8] the authors investigate using RRT* to generate time optimal trajectories through turns that exploit skidding, and avoid the difficulties in general optimization frameworks of the singularities associated with popular tire models at low speeds. However the reported computation times are not low enough for real-time implementations. Williams et al. [9] present a MPC method called model predictive path integral (MPPI) control, a sampling-based algorithm which can optimize for general cost criteria. The MPC algorithm is based on a stochastic optimal control framework, where the optimal controls take the form of a path integral, approximated with an importance sampling scheme. The algorithm is validated on a 1/5 scale Auto-Rally vehicle, at speeds beyond the friction limits of the vehicle.

Velenis et. al introduced a bicycle model with suspension dynamics and applied numerical optimization to analyze drift cornering behavior [10] [11]. They proposed a framework for achieving maximum corner exit velocity or minimal time cornering, and validated their method in CarSim. Voser et al. [12] presented an analytical framework to understand the dynamics of drifting with a simple bicycle model with nonlinear tires, modeling different coefficients of friction between the front and rear tires with the ground. Experimental evidence was collected on a physical all-electric vehicle, P1. Goh et al. [13] presented a controller to drift while tracking

This work was funded in part by NSF NRI award 1526424.

Guillaume Bellegarda and Katie Byl are with the Robotics Laboratory, Department of Electrical and Computer Engineering, University of California at Santa Barbara (UCSB). gbellegarda@ucsb.edu, katiebyl@ucsb.edu

a reference path, using a four-wheel model with steady-state weight transfer, with experimental validation on the physical vehicle MARTY.

Most of the above works decouple planning from control, that is to say, use different models for, as well as separate the processes of, planning and control of a desired motion. Ideally we would want to plan (and then execute) through the same well understood real dynamic model.

Additionally, the tire approximations in the above works all rely on some variant of the linear, Fiala, or Pacejka models [14] [15], which all depend on the tire slip angle. This angle becomes singular at low vehicle speeds due to the vehicle velocity term in the denominator, and is thus difficult to use in a general trajectory optimization framework, additionally so because of the discontinuities in the latter two of these models. The methods discussed above attempt to circumvent this issue with a variety of techniques, from sampling-based methods or scenario-specific optimizations, to using different vehicle models for planning and control.

Contribution: In this work, we explore the feasibility of formulating the contact dynamics of each wheel as a linear complementarity problem with Coulomb friction cone approximations, as introduced by Stewart and Trinkle [16], [17], which has been widely used in robotics applications. This in turn allows for combining planning and control into one process using the same wheel model, for example by formulating and running the trajectory optimization as MPC. In previous work, we explicitly modeled friction forces in this manner for a wheel-legged system on unactuated wheels, where we considered friction acting only perpendicular to a wheel's roll direction, essentially modeling the wheel as an ice skate with a friction triangle [18]. This allowed us to pose the locomotion problem as a whole-body trajectory optimization, which found trajectories that either exploited or avoided skidding depending on the cost function.

To pose the trajectory optimization, as in our previous work [18]–[20], we take direct inspiration from the work done in [21]–[24], where full body control for underactuated systems is achieved via trajectory optimization and stabilization under constraints. [22] in particular introduces an algorithm (DIRCON) that extends the direct collocation method, incorporating manifold constraints to produce nominal trajectories with third-order integration accuracy.

The rest of this paper is organized as follows. Section II describes modeling details for the dynamic bicycle model approximation. Section III describes the trajectory optimization framework used to produce motions, with details and design decisions on the anisotropic Coulomb friction cone model. Experimental results, framework versatility, discussion on model choices, and limitations and future work are considered in Section IV. A brief conclusion is given in Section V.

II. Modeling

As vehicles are modeled in various ways in the literature, and for consistency and completeness, we include the equations of motion for our car system below. The dynamics can be derived via a Lagrangian approach, and we use the bicycle model as our basis. The equations of motion for the system can be written as:

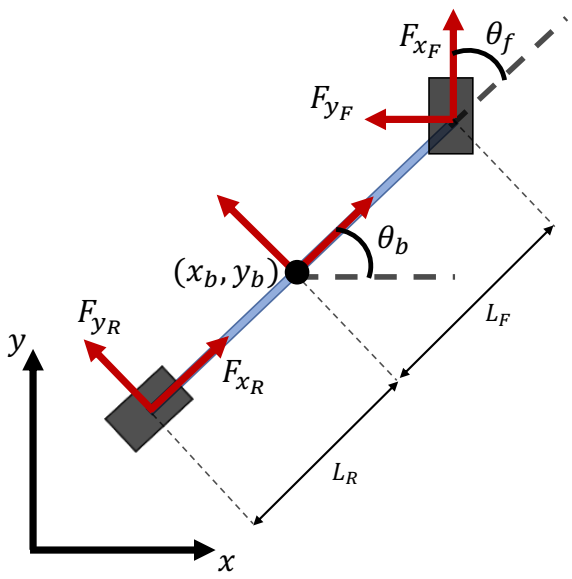

Fig. 1: Dynamic bicycle model.

$$M(q)\ddot{q} + C(q,\dot{q})\dot{q} + G(q) + A(q)^T\lambda = B(q)u + F \quad (1)$$

where q are the generalized coordinates, $M(q)$ is the inertial matrix, $C(q,\dot{q})\dot{q}$ denotes centrifugal and Coriolis forces, $G(q)$ captures potentials (gravity), $A(q)^T\lambda$ are constraint forces (where λ are unknown multipliers a priori), $B(q)$ maps control inputs u into generalized forces, and F contains non-conservative forces such as friction.

For this system, following from Figure 1, $q = [x_b, y_b, \theta_b, \theta_f]^T \in \mathbb{R}^4$. (x_b, y_b) are the global coordinates for the center of mass (COM) of the body, and θ_b represents the counterclockwise (CCW) rotation of the body x-axis, relative to the fixed world frame x-axis x. The steering angle θ_f, relative to body angle θ_b, is not often included as a state in the literature, but instead only as a control input. However, constraints on the angular velocity $\dot{\theta}_f$ and limited steering torque input to the state must be included for realistic motions, motivating our choice of including θ_f.

The body has a point mass m_b and inertia J_b, and each wheel has a point mass, m_1 and m_2, with the front wheel having inertia J_1 about the z-axis (out of the page). Since the COM may not be at the geometric center of the body, we consider the distance from the COM to the center of the front wheel L_F and the distance from the COM to the center of the rear wheel L_R. Frictional forces are considered both in the direction of, and perpendicular to, the direction of wheel roll.

The inertial matrix $M(q)$ can be written as:

$$M(q) = \begin{bmatrix} M_{11} & 0 & M_{13} & 0 \\ 0 & M_{11} & M_{23} & 0 \\ M_{13} & M_{23} & M_{33} & M_{44} \\ 0 & 0 & M_{44} & M_{44} \end{bmatrix} \quad (2)$$

where M_{mn} are as follows:

$$\begin{aligned} M_{11} &= (m_b + m_1 + m_2) \\ M_{13} &= \sin(\theta_b)(m_2 L_R - m_1 L_F) \\ M_{23} &= -\cos(\theta_b)(m_2 L_R - m_1 L_F) \\ M_{33} &= m_2 L_R^2 + m_1 L_F^2 + J_1 + J_b \\ M_{44} &= J_1 \end{aligned}$$

The torques due to centrifugal and Coriolis effects are:

$$C(q,\dot{q})\dot{q} = [C_1, C_2, 0, 0]^{\mathsf{T}} \tag{3}$$

where:

$$\begin{aligned} C_1 &= \dot{\theta}_b^2 \cos(m_2 L_R - m_1 L_F) \\ C_2 &= \dot{\theta}_b^2 \sin(m_2 L_R - m_1 L_F) \end{aligned}$$

The two inputs to the system are a torque to be set at all wheels (All Wheel Drive) in the wheel-rolling directions, and a torque to control the steering angle of the front wheels, or $u = [u_{wheels}, u_{steering}]^T$. These are mapped into generalized coordinates with matrix $B(q)$, defined as:

$$B(q) = \begin{bmatrix} \cos(\theta_b + \theta_f) + \cos(\theta_b) & 0 \\ \sin(\theta_b + \theta_f) + \sin(\theta_b) & 0 \\ L_f \sin(\theta_f) & 0 \\ 0 & 1 \end{bmatrix} \tag{4}$$

If we first define the friction forces in global coordinates as:

$$\begin{bmatrix} F_{x_{Fg}} \\ F_{y_{Fg}} \end{bmatrix} = \begin{bmatrix} \cos(\theta_b + \theta_f) & \sin(\theta_b + \theta_f) \\ -\sin(\theta_b + \theta_f) & \cos(\theta_b + \theta_f) \end{bmatrix} \begin{bmatrix} F_{x_F} \\ F_{y_F} \end{bmatrix}$$

$$\begin{bmatrix} F_{x_{Rg}} \\ F_{y_{Rg}} \end{bmatrix} = \begin{bmatrix} \cos(\theta_b) & \sin(\theta_b) \\ -\sin(\theta_b) & \cos(\theta_b) \end{bmatrix} \begin{bmatrix} F_{x_R} \\ F_{y_R} \end{bmatrix}$$

then F can be written as:

$$F = [F_1, F_2, F_3, 0]^{\mathsf{T}} \tag{5}$$

where

$$\begin{aligned} F_1 &= F_{x_{Fg}} + F_{x_{Rg}} \\ F_2 &= F_{y_{Fg}} + F_{y_{Rg}} \\ F_3 &= -F_{x_{Fg}} L_F \sin(\theta_b) + F_{x_{Rg}} L_R \sin(\theta_b) \\ &\quad + F_{y_{Fg}} L_F \cos(\theta_b) - F_{y_{Rg}} L_R \cos(\theta_b) \end{aligned}$$

The frictional forces will be determined via an anisotropic Coulomb friction cone, to be introduced in Sec. III-D.

A. Note on No-Skid Constraints

For general wheeled mobile robots, $A(q)^T\lambda$ typically contains constraints ensuring no slip (free rolling in the direction the wheel is pointing) and no skid (no velocity along the wheel's rotation axis perpendicular to the free rolling direction), which come from writing these constraints in Pfaffian form $A(q)\dot{q} = 0$. λ can be explicitly solved for by differentiating $A(q)\dot{q} = 0$ and substituting in $\ddot{q}$ from Equation 1. We note that our framework can also find trajectories enforcing these constraints when the assumptions of no slip and no skid are valid, but since we are interested in dynamic maneuvers, for the rest of this paper we set $A(q)^T\lambda = 0$.

III. Trajectory Optimization

This section provides details on formulating the locomotion problem for the system as a trajectory optimization. At a high level, the full nonlinear system is discretized, and direct collocation along with backward Euler integration is used to generate motion as in [18] [21]. More precisely, with slight abuse of notation, the problem is formulated as:

$$\begin{aligned} \text{find} \quad & q, \dot{q}, u, F_n, F_{fric} \text{ at discrete timesteps } k = 1...N && (6) \\ \text{s.t.} \quad & \text{minimize cost } J \text{ (Sec. III-A)} \\ & \text{-State Constraints (Sec. III-B)} \\ & \phi(q,\dot{q},u,F_n) = 0 && (7) \\ & \psi(q,\dot{q},u,F_n) \geq 0 && (8) \\ & \text{-Dynamics Constraints (Sec. III-C)} \\ & M(q)\ddot{q} + C(q,\dot{q})\dot{q} + G(q) \\ & \qquad + A(q)^T\lambda = B(q)u + F_n + J(q)^T F_{fric} && (9) \\ & \text{-Friction Constraints (for each contact } i\text{) (Sec. III-D)} \\ & \gamma e + D^T v^{k+1} \geq 0, \quad \beta \geq 0 && (10) \\ & \mu F_{n_i} - e^T\beta \geq 0, \quad \gamma \geq 0 && (11) \\ & (\gamma e + D^T v^{k+1})^T \beta = 0 && (12) \\ & (\mu F_{n_i} - e^T\beta)\gamma = 0 && (13) \\ & F_{fric_i} = D\beta && (14) \end{aligned}$$

where each of the above constraints is detailed below, along with cost function considerations.

A. Objectives

The cost function J is defined as the weighted squared error between a set of goal coordinates (i.e. a parking space) (x_g, y_g, θ_g) and the body coordinates (x_N, y_N, θ_N), where N is the number of sample points for the trajectory:

$$J = \alpha_x(x_g - x_N)^2 + \alpha_y(y_g - y_N)^2 + \alpha_\theta(\theta_g - \theta_N)^2 \tag{15}$$

where weights $\alpha_x, \alpha_y, \alpha_\theta$ can vary based on the desired task, i.e. if final body orientation is important. Additional terms can be added to minimize final velocities, intermediate states, or energy by penalizing $u^T u$ at each time step.

B. State Constraints

The initial states q and $\dot{q}$ are constrained exactly based on the car's current state. For the rest of the N time points, these are bounded by the feasible work space we are considering and by the physical limits of the car. The input u is also bounded explicitly, as well as implicitly by $\dot{q}$ ranges. We are not explicitly modeling load transfer, but the normal force F_{n_i} at each contact (where $i \in \{1,2\}$) is of large importance as its magnitude directly sets a limit on the frictional force available at each contact point. We investigate the following methods for determining the normal forces:

(1) leaving F_{n_i} as a non-negative open variable
(2) constraining F_{n_i} within "reasonable bounds" (i.e. range in $[1/4(m_b + m_1 + m_2)g,\ (m_b + m_1 + m_2)g]$ at each contact)
(3) setting F_{n_i} as $1/2(m_b + m_1 + m_2)g$

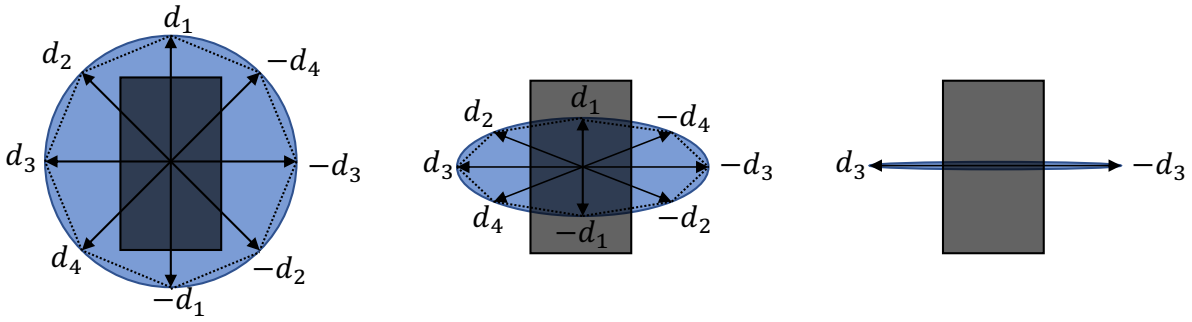

(a) Isotropic friction cone (b) Anisotropic friction cone (c) Triangular friction cone

Fig. 2: (a) Isotropic, (b) anisotropic polyhedral (shown here as octagonal), and (c) triangular friction cone approximations of a contact point at the center of the wheel, when viewed from above. The normal force is coming out of the page, and each arrow represents a direction vector.

Clearly we can expect different results in each of these scenarios, and future work will involve incorporating an accurate load transfer model.

C. Dynamics Constraints

At each time step k, with $h = \Delta t$ the time step interval, the dynamics are constrained:

$$q_{k+1} = q_k + h\dot{q}_{k+1} \tag{16}$$
$$\dot{q}_{k+1} = \dot{q}_k + h\ddot{q}_{k+1} \tag{17}$$

with

$$\ddot{q}_{k+1} = M_{k+1}^{-1}(B_{k+1}u_{k+1} + F_{n_{k+1}} + J_{k+1}^T F_{fric_{k+1}} - C_{k+1}\dot{q}_{k+1} - G_{k+1}) \tag{18}$$

where we write $M(q_{k+1})$ as M_{k+1}, and similar for other terms.

D. Friction as a Linear Complementarity Problem

Determining the friction for each wheel in the optimization is posed as a set of Linear Complementarity Problems (LCPs), and we use the approach detailed by Stewart and Trinkle in [16]. They begin by approximating the circular friction cone by a polyhedral cone $\mathscr{F}$:

$$\mathscr{F}(q) = \{F_n n + D\beta \,|\, F_n \geq 0, \beta \geq 0, e^T\beta \leq \mu F_n\} \tag{19}$$

where F_n is the magnitude of the normal contact force, n is the local unit z-axis representing the six dimensional unit wrench of the normal component of the contact force, the columns of D are direction vectors that positively span the space of possible generalized friction forces, $e = [1,1,...,1]^T \in \mathbb{R}^p$ where p is the number of edges of the polyhedral approximation, and $\beta \in \mathbb{R}^p$ is a vector of weights.

Under Coulomb friction, the frictional force opposes the direction of motion. In our 2D planar car model, this would largely be opposite to the direction of wheel roll, for most behavior, not lending to be very useful for the optimization to produce motions.

Since the physical car is all wheel drive, we can directly input forces in the directions of F_{x_F} and F_{x_R}, and thus set the net force in these directions to overcome any static friction trying to oppose motion in the roll direction. Thus we consider d_1 to be of minimal importance (and in fact set $|d_1| \approx 0$), and consider an anisotropic friction model, as shown in Figure 2.

Intuitively, when driving a car, there is a force perpendicular to a wheel's rolling direction that prevents skidding from occurring under normal circumstances. During aggressive maneuvers however, the body/tire may overcome the static frictional force in this direction, causing a loss of traction and thus skidding. This implies that the magnitude of vector d_3 from Fig. 2 will be most important to plan realistic skidding (or lack thereof) as in the dynamic parking tasks in Sec. IV-B. At this extremity, Fig. 2c in particular shows a triangular friction cone, where friction is modeled only perpendicular to the wheel's roll direction.

For the rest of this paper, we consider two different anisotropic friction models:

(1) $|d_1| = |d_2| = |d_4| = 0$, $|d_3| = 1$ (Fig. 2c)
(2) $|d_1| = 0.01, |d_2| = |d_4| = 0.3$, $|d_3| = 1$ ($\sim$Fig. 2b)

1) LCP Formulation: For each contact at each time step, the following inequality constraints are enforced to produce the correct friction forces:

$$\gamma e + D^T v^{k+1} \geq 0, \quad \beta \geq 0 \tag{20}$$
$$\mu F_n - e^T\beta \geq 0, \quad \gamma \geq 0 \tag{21}$$

with the complementarity conditions:

$$(\gamma e + D^T v^{k+1})^T \beta = 0 \tag{22}$$
$$(\mu F_n - e^T\beta)\gamma = 0 \tag{23}$$

where γ can be interpreted as a scalar roughly equal to the magnitude of the relative tangential velocity at a contact, and v^{k+1} is the global 2D planar velocity vector of the contact point at the end of the next time step. From the above constraints the friction F_{fric} at a particular contact can then be recovered with:

$$F_{fric} = \begin{bmatrix} F_{fric_x} \\ F_{fric_y} \end{bmatrix} = D\beta \tag{24}$$

F_{fric} for each contact is then mapped from global coordinates to generalized coordinates with $J(q)^T$ and input into Equation 9.

IV. Results

A. Implementation Details

The trajectory optimization is implemented in MATLAB with CasADi [25], using IPOPT [26] to solve the NLP. The car hardware is an Exceed RC Blaze model, which is an All Wheel Drive (AWD) vehicle. A Raspberry Pi with a Navio2 board is used to interface with the motor and steering servo. The forces found with the optimization are converted to PWM signals to send to the motor and servo.

The car parameters are shown in Table I. The masses and distances are measured, and inertias are estimated from the masses and physical dimensions of the relevant components. The COM is estimated to be at the geometric center of the vehicle, and the coefficient of friction is estimated from the material properties.

B. Dynamic Skidding Parking Maneuver

We illustrate the effectiveness of our method by considering two different dynamic drift parking scenarios. The reader is encouraged to watch the accompanying video for better visualizations.

In the first scenario, shown in Figure 3, the car starts from rest at $(x_0, y_0) = (0,0)$ with body angle $\theta_0 = 0$. The cost function penalizes deviations from the goal location of $(x_N, y_N) = (2.5, 0)$ with body angle $\theta_N = \pi/2$, under a short planning horizon of $T = 0.75$ (s), where $N = 15$. The anisotropic friction model used is (1) from Sec. III-D, and the normal forces are as (2) in Sec. III-B (though we note (3) produces reasonable results as well). The result is a forward sliding parking maneuver with a 90-degree turn.

In the second scenario, shown in Figure 4, the car starts from rest at $(x_0, y_0) = (0,0)$ but with body angle $\theta_0 = -\pi$. The cost function penalizes deviations from the goal location of $(x_N, y_N) = (2, 0.8)$ with body angle $\theta_N = 0$, under a short planning horizon of $T = 1$ (s), where $N = 20$. The anisotropic friction model used is (2) from Sec. III-D, and the normal forces are as (2) in Sec. III-B, (though we note (3) produces reasonable results as well). The result is a 180-degree backward sliding parking maneuver.

For both of these scenarios under such short planning horizons, it is not physically possible to achieve either goal without skidding. The snapshots in the figures are the result of open-loop execution of the trajectory found with the optimization framework, and we could expect better tracking performance if using a mixed open-loop closed-loop controller such as in [4] or [5].

Since the trajectories are executed open-loop, any slight offsets at the start of the trajectory, in addition to unmodeled states such as the motor or gear backlash, will have a large effect on the final body position. Figure 5 shows the final body position for executing 21 open-loop trials of the forward park skidding task. However, the distance traveled always remains roughly the same, as well as the final body angle of $\pi/2$, where differences in the final body y position result from the initial heading errors and compounding effects from hidden states.

Parameter	Value
m_b [kg]	1.26
m_1 [kg]	0.01
m_2 [kg]	0.01
L_F [m]	0.09
L_R [m]	0.09
J_b [kg $\cdot$ m^2]	0.0064
J_1 [kg $\cdot$ m^2]	3.5E-6
μ	0.7

TABLE I: Car and environment physical parameters.

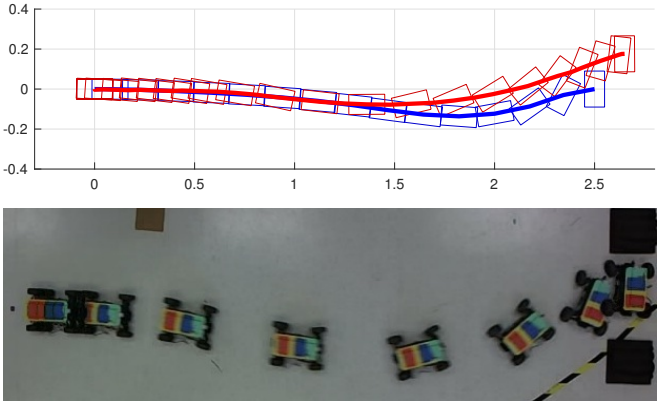

Fig. 3: Forward park skidding.

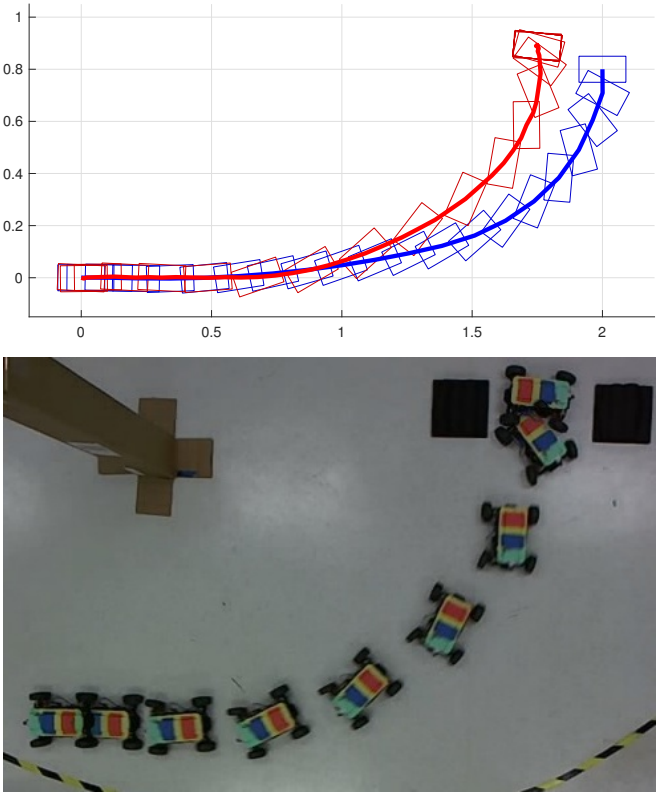

Fig. 4: Backward park skidding.

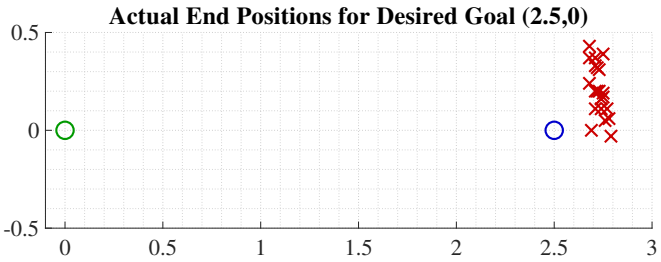

Fig. 5: End position error across 21 trials for the forward park skidding task.

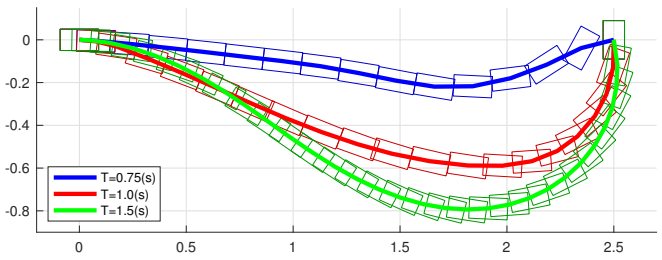

Fig. 6: Trajectories found for horizons of 0.75 (s), 1.0 (s), and 1.5 (s) (with N=15,20,30, respectively) where the cost function penalizes distance from $(x_{b_N}, y_{b_N}, \theta_{b_N}) = (2.5, 0, \pi/2)$. For the shortest planning horizon, skidding is required in order to minimize the cost function and reach the goal.

C. Versatility of Framework

In section IV-B we showed two examples of dynamic trajectories found with our framework under short planning horizons, where we noted that skidding was required in order to minimize the cost function. However, we would also like to note the versatility of our framework as we consider longer planning horizons for the same tasks. Figure 6 shows three locally optimal trajectories found by our framework for the forward skidding parking task over planning horizons of 0.75, 1.0, and 1.5 seconds. The cost function is still minimizing the difference between the Nth (last) knot point and the goal in all three trajectories. As the planning horizon lengthens, skidding is no longer required to achieve the goal, and our framework finds a longer, slower path that minimizes the cost function. This shows that the anisotropic friction model in conjunction with our framework can produce intuitive and realistic trajectories regardless of vehicle velocity, and can be used as a general tool including non-drifting scenarios.

D. Discussion

One point warranting further discussion and future work is the direction vectors that make up the matrix D for the anisotropic Coulomb friction cone approximation. Experimentally we found that the vectors perpendicular to the roll direction are most important to capture the true dynamics and produce feasible trajectories, both for the optimization and evaluation on the real system. Future work will investigate if we can empirically fit the magnitudes of the direction vectors D, similar in spirit to the system identification approach often used with the Pacejka tire model.

Another point of discussion is the magnitude of the normal force. In this paper we did not model load transfer, but considered evenly distributing the normal force between the front and rear wheels, or leaving it as a lightly/positively-constrained variable in the optimization. The problem with the former is that it does not model load transfer, which may result in unnecessarily conservative or inaccurate trajectories. The problem with the latter is that this lets the optimization choose a friction force with essentially any magnitude, or in unrealistic ranges, which can produce unrealistic trajectories. Future work will explore accurate normal force modeling, perhaps involving modeling additional states.

V. Conclusion

In this work, we have considered modeling vehicle tire dynamics as an anisotropic Coulomb friction cone. This allows us to formulate the tire dynamics as a linear complementarity problem and optimize over all states and forces, producing realistic motions that may or may not include drifting behavior, depending on the planning horizon and cost function. Notably, this wheel model avoids the singularities at low speeds of other popular tire models, and allows planning and control through the same tire model. We verified the resulting trajectories on a 1/16 scale model car, and discussed extensions for further validating the anisotropic friction cone as a useful vehicle tire model.

References

[1] F. Borrelli, P. Falcone, T. Keviczky, J. Asgari, and D. Hrovat, "Mpc-based approach to active steering for autonomous vehicle systems," 2005.

[2] J. Kong, M. Pfeiffer, G. Schildbach, and F. Borrelli, "Kinematic and dynamic vehicle models for autonomous driving control design," in *2015 IEEE Intelligent Vehicles Symposium (IV)*, June 2015, pp. 1094–1099.

[3] J. Kabzan, M. de la Iglesia Valls, V. Reijgwart, H. F. C. Hendrikx, C. Ehmke, M. Prajapat, A. Bhler, N. Gosala, M. Gupta, R. Sivanesan, A. Dhall, E. Chisari, N. Karnchanachari, S. Brits, M. Dangel, I. Sa, R. Dub, A. Gawel, M. Pfeiffer, A. Liniger, J. Lygeros, and R. Siegwart, "Amz driverless: The full autonomous racing system," 2019.

[4] J. Z. Kolter, C. Plagemann, D. T. Jackson, A. Y. Ng, and S. Thrun, "A probabilistic approach to mixed open-loop and closed-loop control, with application to extreme autonomous driving," in *2010 IEEE International Conference on Robotics and Automation*, May 2010, pp. 839–845.

[5] E. Jelavic, J. Gonzales, and F. Borrelli, "Autonomous drift parking using a switched control strategy with onboard sensors," *IFAC-PapersOnLine*, vol. 50, no. 1, pp. 3714 – 3719, 2017, 20th IFAC World Congress. [Online]. Available: http://www.sciencedirect.com/science/article/pii/S2405896317309394

[6] F. Zhang, J. Gonzales, K. Li, and F. Borrelli, "Autonomous drift cornering with mixed open-loop and closed-loop control," *IFAC-PapersOnLine*, vol. 50, no. 1, pp. 1916 – 1922, 2017, 20th IFAC World Congress. [Online]. Available: http://www.sciencedirect.com/science/article/pii/S2405896317305803

[7] F. Zhang, J. Gonzales, S. E. Li, F. Borrelli, and K. Li, "Drift control for cornering maneuver of autonomous vehicles," *Mechatronics*, vol. 54, pp. 167 – 174, 2018. [Online]. Available: http://www.sciencedirect.com/science/article/pii/S0957415818300771

[8] J. h. Jeon, S. Karaman, and E. Frazzoli, "Anytime computation of time-optimal off-road vehicle maneuvers using the rrt*," in *2011 50th IEEE Conference on Decision and Control and European Control Conference*, Dec 2011, pp. 3276–3282.

[9] G. Williams, P. Drews, B. Goldfain, J. M. Rehg, and E. A. Theodorou, "Aggressive driving with model predictive path integral control," in *2016 IEEE International Conference on Robotics and Automation (ICRA)*, May 2016, pp. 1433–1440.

[10] E. Velenis and P. Tsiotras, "Minimum time vs maximum exit velocity path optimization during cornering," in *Proceedings of the IEEE International Symposium on Industrial Electronics, 2005. ISIE 2005.*, vol. 1, June 2005, pp. 355–360.

[11] E. Velenis, D. Katzourakis, E. Frazzoli, P. Tsiotras, and R. Happee, "Steady-state drifting stabilization of rwd vehicles," *Control Engineering Practice*, vol. 19, no. 11, pp. 1363 – 1376, 2011. [Online]. Available: http://www.sciencedirect.com/science/article/pii/S0967066111001614

[12] C. Voser, R. Y. Hindiyeh, and J. C. Gerdes, "Analysis and control of high sideslip manoeuvres," *Vehicle System Dynamics*, vol. 48, no. sup1, pp. 317–336, 2010. [Online]. Available: https://doi.org/10.1080/00423111003746140

[13] J. Y. Goh and J. C. Gerdes, "Simultaneous stabilization and tracking of basic automobile drifting trajectories," in *2016 IEEE Intelligent Vehicles Symposium (IV)*, June 2016, pp. 597–602.

[14] H. Pacejka, *Tire and vehicle dynamics*. Elsevier, 2005.

[15] H. B. Pacejka and E. Bakker, "The magic formula tyre model," *Vehicle System Dynamics*, vol. 21, no. sup001, pp. 1–18, 1992. [Online]. Available: https://doi.org/10.1080/00423119208969994

[16] D. E. Stewart and J. C. Trinkle, "An implicit time-stepping scheme for rigid body dynamics with Coulomb friction," in *Proc. IEEE Int. Conf. on Robotics and Automation (ICRA)*, 2000, pp. 162–169. [Online]. Available: https://doi.org/10.1109/ROBOT.2000.844054

[17] ——, "An implicit time-stepping scheme for rigid body dynamics with inelastic collisions and coulomb friction," *International Journal for Numerical Methods in Engineering*, vol. 39, no. 15, pp. 2673–2691, 1996. [Online]. Available: https://onlinelibrary.wiley.com/doi/abs/10.1002/%28SICI%291097-0207%2819960815%2939%3A15%3C2673%3A%3AAID-NME972%3E3.0.CO%3B2-I

[18] G. Bellegarda and K. Byl, "Trajectory optimization for a wheel-legged system for dynamic maneuvers that allow for wheel slip," in *2019 IEEE International Conference on Decision and Control (CDC), in Press*.

[19] G. Bellegarda, N. Talele, and K. Byl, "Nonintuitive optima for dynamic locomotion: The Acrollbot," in *IEEE Int. Conf. on Robotics and Automation (ICRA)*, May 2018, pp. 3130–3136.

[20] G. Bellegarda and K. Byl, "Combining benefits from trajectory optimization and deep reinforcement learning," *arXiv preprint arXiv:1910.09667*, 2019.

[21] M. Posa and R. Tedrake, "Direct trajectory optimization of rigid body dynamical systems through contact," in *Algorithmic foundations of robotics X*. Springer Tracts in Adv. Robotics, 2013, pp. 527–542.

[22] M. Posa, S. Kuindersma, and R. Tedrake, "Optimization and stabilization of trajectories for constrained dynamical systems," in *Proc. IEEE International Conference on Robotics and Automation (ICRA)*. IEEE, 2016, pp. 1366–1373.

[23] M. Posa, C. Cantu, and R. Tedrake, "A direct method for trajectory optimization of rigid bodies through contact," *International Journal of Robotics Research*, vol. 33, no. 1, pp. 69–81, 2014.

[24] S. Feng, E. Whitman, X. Xinjilefu, and C. G. Atkeson, "Optimization-based full body control for the DARPA Robotics Challenge," *Journal of Field Robotics*, vol. 32, no. 2, pp. 293–312, 2015.

[25] J. A. E. Andersson, J. Gillis, G. Horn, J. B. Rawlings, and M. Diehl, "CasADi – A software framework for nonlinear optimization and optimal control," *Mathematical Programming Computation*, vol. 11, no. 1, pp. 1–36, 2019.

[26] A. Wächter and L. T. Biegler, "On the implementation of an interior-point filter line-search algorithm for large-scale nonlinear programming," *Mathematical Programming*, vol. 106, no. 1, pp. 25–57, Mar 2006. [Online]. Available: https://doi.org/10.1007/s10107-004-0559-y